Inorganic Chemistry

Article

pubs.acs.org/IC

From 1D Helix to 0D Loop: Nitrite Anion Induced Structural Transformation Associated with Unexpected *N*-Nitrosation of Amine Ligand

Jing-Yun Wu,*[,†] Yu-Chiao Liu,[‡] and Tzu-Ching Chao[†]

[†]Department of Applied Chemistry, National Chi Nan University, 1 University Road, Puli, Nantou 545, Taiwan

[‡]Institute of Chemistry, Academia Sinica, 128 Academia Road, Section 2, Nankang, Taipei 115, Taiwan

Supporting Information

ABSTRACT: An infinite Ag(I) coordination 4_1-helical chain, $[Ag(Hdpma)](NO_3)_2{\cdot}H_2O$ (**1**), was synthesized by the self-assembly of $AgNO_3$ and di(3-pyridylmethyl)amine (dpma). Helix **1** is 5-fold interweaved and has a topological diamondoid-like net that is extended by ligand-unsupported helix-to-helix argentophilic interactions. Two identical diamondoid-like nets with opposite chiralities interpenetrate to form the whole 3D framework as a meso compound. Typical anion-exchange reactions cause a remarkable single-crystal-to-single-crystal (SCSC) structural transformation from the 1D helix **1** to the 0D molecular loop $[Ag(dpma\text{-}NO)(NO_2)]_2$ (**2**) (induced by the nitrite anion, NO_2^-) and a 1D molecular ladder $[Ag(dpma)(H_2O)](NO_3)$ (induced by the fluoride anion, F^-). Molecular loop **2** is an *N*-nitroso compound. This work is the first to present observations of nitrite-dominated in situ *N*-nitrosation of an amine ligand which accompanies SCSC structural transformation via an anion-exchange reaction.

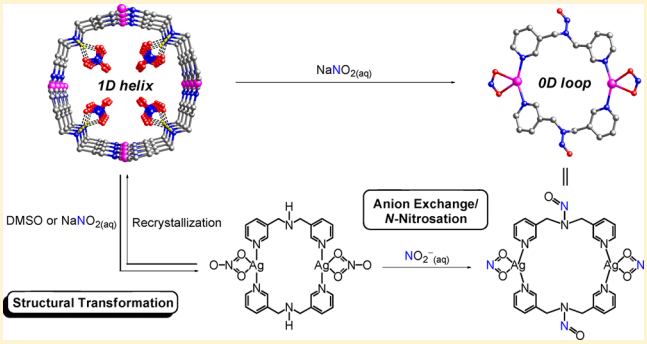

INTRODUCTION

The variety of coordination-driven infinite networks of metal ions/clusters and polytopic bridging ligands has been extensively studied owing to not only their intriguing structural diversity but also their capacities for gas sorption, ion exchange, separation, heterogeneous catalysis, and chemical sensing.[1,2] One major interest concerning many polymeric metal−organic networks is their helical crystal structures because they enable the mimicking of complex biological processes and their application to enantioselective processes, such as chiral sensing (recognition and separation) and asymmetric catalysis.[3] Many infinite coordination helical structures (1D helical chains, 2D sheets, and 3D frameworks) with single-, double-, or multi-stranded helices have been fabricated by metal−ligand coordination interactions, hydrogen-bonding, $\pi-\pi$ stacking, and argentophilic interactions by using enantiopure, racemic, or achiral molecules as building blocks.[4] The resultant helical structures in the crystalline phase are a chiral/enantiopure product (chiral single crystals), a meso compound (achiral single crystals that are composed of equal amounts of opposite-handedness chiral networks), or a conglomerate (racemic mixture of chiral single crystals), and in a very few cases, a nonzero enantiomeric excess product (nonracemic mixture of chiral single crystals).[4a,b]

Ion exchange, an early recognized function of coordination polymers,[5] has been widely investigated because of its potential usefulness in trapping/detecting specific ions and releasing/sequestering guest ions that are very important for environment cleaning and food security.[6,7] Interestingly, ion exchange that occurs in coordination polymers is usually accompanied by single-crystal-to-single-crystal (SCSC) structural transformation,[5d,8] principally because these metal−organic networks have several distinct polymeric architectures in response to external stimuli. For example, an ideal helical spring, constructed from skewed conformational units with nonrigid interannular dihedral angles, has a helical pitch that can be reversibly stretched by counteranion exchange.[5d] In addition to ion exchange, the induction of characteristic crystal transformations depends on the removal or exchange of guest and solvent molecules and some physical stimuli such as light, heat, acido-basicity, or mechanochemical force, and even an exchange of chemical constituents such as metal ions and bridging ligands.[9] The three structural transformations that have been observed involve maintenance of the host-framework without any change in the network topology, deformation of the host-framework from the mother structure, and rearrangement of host-framework into a new network topology.[10] The first transformation yields a final network that is structurally similar to the initial network while the latter two involve remarkably distinct structural conversions.

Received: February 6, 2014
Published: May 21, 2014

   dx.doi.org/10.1021/ic500306y | *Inorg. Chem.* 2014, 53, 5581−5588

N-Nitrosamines are important in synthesis and biology.[11,12] As is well-known, *N*-nitrosamines are useful synthetic intermediates in the synthesis of various *N*,*N*-bonded functionalities, and they can be utilized in the regio- and stereoselective substitution of the secondary amines at the α-carbon by reactions with electrophiles.[11,13] The latter results from the restricted N—NO rotation due to the partial double-bond nature in the N—NO bond that is formed by the partition of p electrons on nitrogen to the N═O π-system.[11,13a,14] Additionally, *N*-nitrosamines are usually considered as strong mutagens and carcinogens[12c,d,13a] and can be shown to be potential donors of nitric oxide ($NO^{\bullet}$), a messenger in cellular signaling,[15] and of nitrosonium ion (NO^{+}) by the homolytic or heterolytic cleavage of the N—NO bond, respectively.[11,16] This study presents a novel inorganic supramolecular system that exhibits an interesting nitrite anion-induced structural transformation from a 1D helix to a 0D molecular loop, which is associated with the unexpected in situ *N*-nitrosation of amine ligand.

EXPERIMENTAL SECTION

Materials and Instruments. Ligand di(3-pyridylmethyl)amine (dpma) was prepared following a published procedure.[17,18] Other chemicals were used as received from commercial sources. ^{1}H NMR spectra were collected at room temperature on a Bruker AMX-300, an AV-400, and a DRX-500 spectrometers operating at 300, 400, and 500 MHz, respectively. $^{13}C\{^{1}H\}$ spectra were collected on either a DRX-500 or a AV-500 spectrometer operating at 125.7 MHz. $^{15}N\{^{1}H\}$ NMR spectra were collected on a AV-500 spectrometer operating at 50.5 MHz. Spectra were obtained in DMSO-d_6. Chemical shifts are reported in parts per million (ppm), and coupling constants are reported in hertz (Hz). ^{1}H NMR spectra were referenced to the residual protiosolvent peak at 2.50 ppm. $^{15}N\{^{1}H\}$ NMR spectra were obtained with inverse gated proton decoupling and referenced to external nitromethane ($MeNO_2$, 0 ppm). Electrospray ionization (ESI) mass spectra were carried out on a Waters LCT Premier XE mass spectrometer combined with the ESCi (ESI/APCi) dual-mode ionization source at the Mass Spectrometry Center in the Institute of Chemistry, Academia Sinica. Infrared (IR) spectra were recorded on a PerkinElmer Frontier Fourier transform infrared spectrometer using attenuated total reflection (ATR) technique. Thermogravimetric analysis measurements were conducted on a Thermo Cahn VersaTherm HS TG analyzer under a flux of nitrogen. X-ray powder diffraction (XRPD) patterns were acquired on a Siemens D-5000 diffractometer with graphite monochromatized Cu Kα (λ = 1.5406 Å; 40 kV, 30 mA) at a scan speed of 1.2° min^{-1}. Scanning electron microscopy (SEM) images were obtained by using a Carl Zeiss ULTRA plus FE-SEM instrument. Photoluminescent measurements were conducted on a Hitachi F4500 fluorescence spectrophotometer in the solid-state at room temperature. Microanalyses (C, H, N) were carried out with an Elementar Vario EL III elemental analyzer.

Synthesis of [Ag(Hdpma)](NO$_3$)$_2$·H$_2$O (1). In a test tube, ligand dpma (39.8 mg, 0.20 mmol) in MeOH (5 mL) was carefully layered onto an aqueous solution (5 mL) of $AgNO_3$ (33.9 mg, 0.20 mmol) and conc HNO_3 (1 drop), with a mixture of MeOH and H_2O (6 mL, 1:1 v/v, middle) as a buffer, at room temperature. The solutions were left to quietly stand for about 2 weeks at room temperature, and colorless cube-like crystals were obtained (36.0 mg, yield 40%). Anal. Calcd for $C_{12}H_{16}AgN_5O_7$: C, 32.02; H, 3.59; N, 15.56%. Found: C, 32.42; H, 3.90; N, 15.46%. IR (ATR, cm^{-1}): 3483b, 3087w, 1610m, 1456w, 1433m, 1355m, 1326s, 1296s, 1233w, 1193m, 1131w, 1111w, 1057w, 1035m, 968m, 944w, 813m, 705s.

Anion Exchange of 1 with NaNO$_2$. A polycrystalline sample of **1** (44.2 mg) was immersed in an aqueous solution (5 mL) of excess (10 equiv) $NaNO_2$ at room temperature. The solutions were left to quietly stand for about 7 days. The reaction mixture was filtered and then washed with distilled water. The colorless granule-shaped crystal was characterized as $[Ag(dpma\text{-}NO)(NO_2)]_2$ (**2**) by single-crystal X-ray diffraction. Yield 58% (22.0 mg). Anal. Calcd for $C_{24}H_{24}Ag_2N_{10}O_6$: C, 37.72; H, 3.17; N, 18.33%. Found: C, 37.55; H, 3.89; N, 18.75%. ^{1}H NMR (500 MHz, DMSO-d_6): δ 8.56 (s, 2H), 8.51 (d, J = 5.0 Hz, 2H), 8.39 (d, J = 5.0 Hz, 2H), 8.26 (s, 2H), 7.71 (d, J = 7.5 Hz, 2H), 7.40 (d, J = 7.5 Hz, 2H), 7.37 (dd, J = 7.5, 5.0 Hz, 2H), 7.25 (dd, J = 7.5, 5.0 Hz, 2H), 5.48 (s, 4H), 4.74 (s, 4H) ppm. $^{13}C\{^{1}H\}$ NMR (125.7 MHz, DMSO-d_6): δ 150.127, 149.966, 149.667, 149.023, 136.758, 136.202, 131.501, 130.745, 124.303, 123.955, 53.614, 45.409 ppm. ESI-MS (M = $C_{24}H_{24}(^{14}N)_{10}O_6Ag_2$ = 764.2): m/z 870.9 $[M + Ag]^+$ (870.9), 785.0 $[M + Na]^+$ (787.0), 718.0 $[M - NO_2]^+$ (718.0), 563.1 $[M - 2NO_2 - Ag]^+$ (563.1), 489.9 $[M - NO_2 - (dpma\text{-}NO)]^+$ (489.9), 460.9 $[M - NO_2 - (dpma\text{-}NO) - NO + H]^+$ (460.9), 335.0 $[M/2 - NO_2]^+$ (335.0), 305.0 $[M/2 - NO_2 - NO]^+$ (305.0). IR (ATR, cm^{-1}) for $[Ag(dpma\text{-}NO)(NO_2)]_2$ (**2**): 3105w, 3083w, 3057w, 3019w, 2991w, 2970w, 1601m, 1582w, 1485m, 1456w, 1434s, 1382w, 1372w, 1329m, 1303m, 1195s, 1168w, 1142w, 1122m, 1100w, 1052m, 1032m, 971m, 942m, 843m, 828w, 797m, 700s.

^{15}N-Labeled *N*-nitroso compound $[Ag(dpma\text{-}^{15}NO)(^{15}NO_2)]_2$ (**2′**) was obtained by a similar synthetic procedure for preparing **2**, with the use of $Na^{15}NO_2$ instead of $NaNO_2$. $^{15}N\{^{1}H\}$ NMR (50.5 MHz, DMSO-d_6): δ 158.951 (NO), 210.017 (NO_2) ppm. ESI-MS (M = $C_{24}H_{24}(^{14}N)_6(^{15}N)_4O_6Ag_2$ = 768.0): m/z 874.9 $[M + Ag]^+$ (874.9), 721.0 $[M - (^{15}NO_2)]^+$ (721.0), 565.1 $[M - 2(^{15}NO_2) - Ag]^+$ (565.1), 491.9 $[M - (^{15}NO_2) - (dpma\text{-}^{15}NO)]^+$ (491.9), 461.9 $[M - (^{15}NO_2) - (dpma\text{-}^{15}NO) - (^{15}NO) + H]^+$ (461.9), 336.0 $[M/2 - (^{15}NO_2)]^+$ (336.0), 307.0 $[M/2 - (^{15}NO_2) - (^{15}NO)]^+$ (305.0). IR (ATR, cm^{-1}) for $[Ag(dpma\text{-}^{15}NO)(^{15}NO_2)]_2$ (**2′**): 3104w, 3082w, 3056w, 3021w, 2989w, 1600m, 1582w, 1485m, 1431s, 1410m, 1380w, 1365w, 1326m, 1298m, 1177s, 1120m, 1098m, 1051m, 1032m, 968m, 940m, 843w, 797m, 701s.

Intermediate [Ag(dpma)(NO$_3$)]$_2$ (I). A polycrystalline sample of **1** (44.2 mg) was immersed in an aqueous solution (5 mL) of excess (10 equiv) $NaNO_2$ at room temperature. The solution was allowed to quietly stand for approximately 3 h, and then filtered off. The resulting powdered samples were filtered and washed by distilled water several times and, then, used for spectroscopic characterizations. ^{1}H NMR (400 MHz, DMSO-d_6, ppm): δ 9.29 (br, d, J = 8.0 Hz, 2H), 8.65 (d, J = 1.6 Hz, 4H), 8.60 (dd, J = 4.8, 1.2 Hz, 4H), 7.92 (dd, J = 9.6, 1.6 Hz, 4H), 7.49 (dd, J = 8.0, 4.8 Hz, 4H), 4.26 (s, 8H). $^{13}C\{^{1}H\}$ NMR (125.7 MHz, DMSO-d_6, ppm): δ 151.530, 150.689, 138.579, 128.515, 124.233, 48.355. ESI-MS (M = $C_{24}H_{26}(^{14}N)_8O_6Ag_2$ = 738.0): m/z: 844.9 $[M + Ag]^+$ (844.9), 676.0 $[M - NO_3]^+$ (676.0), 507.1 $[M - 2NO_3 - Ag]^+$ (505.1), 476.9 $[M - NO_3 - dpma]^+$ (476.9), 306.0 $[M/2 - NO_3]^+$ (306.0). IR (ATR, cm^{-1}) for $[Ag(dpma)(NO_3)]_2$ (**I**): 3477b, 3087w, 3047w, 1607m, 1432s, 1356s, 1324s, 1300s, 1193w, 1130w, 1111w, 1035m, 968m, 812s, 706s, 651w. Recrystallization of the powdered samples in water formed colorless granule-shaped crystals suitable for single-crystal X-ray diffraction which confirmed the regeneration of helix **1**.

Anion Exchange of 1 with Tetra-*n*-butylammonium Fluoride (TBAF). A polycrystalline sample of **1** (44.2 mg) was immersed in an aqueous solution (5 mL) of excess (10 equiv) TBAF at room temperature. The solutions were left to quietly stand for about 7 days. The reaction mixture was filtered and then washed with distilled water. The colorless granule-shaped crystals were characterized as $[Ag(dpma)(H_2O)](NO_3)$[18] by X-ray crystallography (single-crystal X-ray diffraction and X-ray powder diffraction, see Supporting Information Figure S21).

Crystallographic Determination. Data collection for **1** was performed at 296(2) K within the limits of $2.42° \le \theta \le 25.04°$ on a Bruker Smart CCD-based diffractometer equipped with a graphite monochromated Mo Kα radiation (λ = 0.710 73 Å). Data for **2** were collected at 110(2) K within the limits of $2.88° \le \theta \le 29.16°$ by using an Oxford Diffraction Gemini S diffractometer. The structures were solved by direct methods with SHELXS-97[19] for **1** and SIR92[20] for **2**. Both of the structures were refined by the full-matrix least-squares method on F^2 using the WINGX[21] and SHELX-97[19] program packages. Anisotropical thermal factors were assigned to non-hydrogen atoms except solvent molecules in **1**. Generally, the positions of the

dx.doi.org/10.1021/ic500306y | Inorg. Chem. 2014, 53, 5581−5588

C−H hydrogen atoms were generated geometrically and were assigned isotropic thermal parameters. The positions of the N−H and O−H hydrogen atoms were structurally evident in difference Fourier maps and refined isotropically. For **1**, there are electron residuals in the voids attributed to the solvent molecules that would be reasonably modeled as two partial-occupied water molecules. The lattice water molecule O4 lay on a special position, with a site occupancy factor of 0.25, whereas the lattice water molecule O5 lay on a general position, with a site occupancy factor of 0.25. Both of them were refined isotropically. For **2**, the *N*-nitrosamine oxygen was disordered over two positions with site occupancy factors of 0.60 (O3) and 0.40 (O3′), respectively, which leads to a short contact between the two disordered oxygen atoms. All of the crystal data and structure refinement details are summarized in Table 1. CCDC 983045 and 983046 contain the supplementary crystallographic data for this Article.

Table 1. Crystallographic Data for 1 and 2

	1	2
empirical formula	$C_{12}H_{16}AgN_5O_7$	$C_{24}H_{24}Ag_2N_{10}O_6$
M_w	450.17	764.27
cryst syst	tetragonal	triclinic
space group	$I4_1/acd$	$P\bar{1}$
a (Å)	15.9325(6)	7.9739(4)
b (Å)	15.9325(6)	8.4019(4)
c (Å)	25.3047(10)	11.2669(6)
α (deg)	90	82.796(4)
β (deg)	90	71.409(4)
γ (deg)	90	68.115(4)
V (Å^3)	6423.5(4)	663.87(6)
Z	16	1
T (K)	296(2)	110(2)
λ (Å)	0.710 73	0.710 73
D_{calc} (g cm^{-3})	1.862	1.912
F_{000}	3616	380
μ (mm^{-1})	1.304	1.537
θ_{min}, θ_{max} (deg)	2.42, 25.04	2.88, 29.16
reflns collected	10 886	6070
unique reflns (R_{int})	1413 (R_{int} = 0.0199)	3080 (R_{int} = 0.0282)
obsd reflns ($I > 2\sigma(I)$)	1210	2702
params	116	199
R1[a] ($I > 2\sigma(I)$)	0.0254	0.0318
wR2[b] ($I > 2\sigma(I)$)	0.0628	0.0580
R1[a] (all data)	0.0308	0.0400
wR2[b] (all data)	0.0662	0.0609
GOF on F^2	1.062	1.037
$\Delta\rho_{max}$, $\Delta\rho_{min}$ (e Å^{-3})	0.273, −0.286	0.612, −0.452

[a] $R1 = \sum||F_o| - |F_c||/\sum|F_o|$. [b] $wR2 = \{\sum[w(F_o^2 - F_c^2)^2]/\sum[w(F_o^2)^2]\}^{1/2}$.

RESULTS AND DISCUSSION

Compound $[Ag(Hdpma)](NO_3)_2{\cdot}H_2O$ (**1**) was prepared as colorless cube-like crystals by the diffusion of a methanol solution of di(3-pyridylmethyl)amine (dpma) into an aqueous solution of $AgNO_3/HNO_3$ with a 1:1 mixture of MeOH and H_2O as a buffer. Single-crystal X-ray diffraction analysis revealed that compound **1** crystallizes in the tetragonal space group $I4_1/acd$. The asymmetric unit contains half of a silver atom, half of a protonated Hdpma ligand, one nitrate anion, a quarter of a lattice water molecule lay on a special position, and a quarter of a lattice water molecule lay on a general position. The Ag atom is coordinated by two symmetry-related trans−trans−anti configured Hdpma ligands, with a $C_{py}-C-N_{am}-C$ torsion angle of 179.6°, in an approximately linear fashion, with $N_{py}-Ag-N_{py}$ = 173.34(11)°, to form a one-dimensional Ag−Hdpma helical chain structure that runs along the crystallographic 4_1 screw axis in the c direction with a pitch of 25.30 Å (Figure 1a,b). These 4_1-helices with the same chirality are 5-fold interweaved and further locked by ligand-unsupported helix-to-helix argentophilic interactions (Ag···Ag, 3.0679(6) Å, Figure 1c,d). However, each 4_1-helix is also surrounded by four 4_1-helical chains of opposite chirality, and notably, no two closed opposite-handed 4_1-helices interweave (Supporting Information Figure S3). The nitrate anion adopts a chelating mode to weakly interact with the Ag atom (since that the Ag···O_3N distances of 2.92 and 2.95 Å are significantly shorter by ~0.3 Å than the sum (3.24 Å)[22] of r_{vdW}(Ag) and r_{vdW}(O), where r_{vdW} = van der Waals radius), and also forms pertinent hydrogen-bonding interactions with the ammonium hydrogens in the Hdpma ligands (N1−H101···O2, 2.992(6) Å, Supporting Information Figure S4). Topologically, the Ag_2 units can be treated as tetrahedral junctions and the Hdpma ligands as linear linkers (Supporting Information Figure S5a), making the extended network a diamondoid-like net (Supporting Information Figure S5b). Such a single chiral network has open channels (Figure 2a and Supporting Information Figure S6). When viewed along the crystallographic a (or b) axis, the open channel has dimensions of approximately 5.7 × 6.3 Å^2 (Supporting Information Figure S6b), when the van der Waals radii of the constituent atoms are considered. Two such

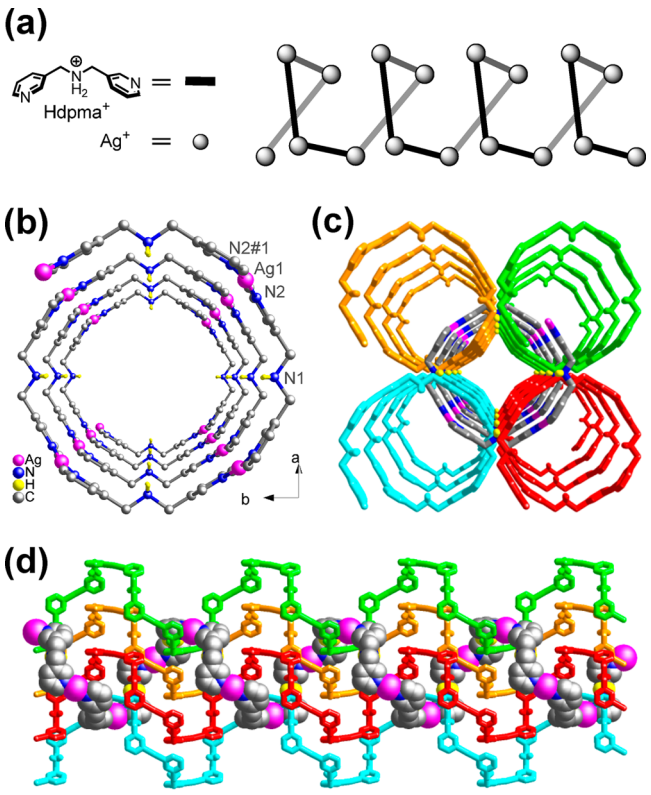

Figure 1. Crystal structure of **1**. (a) Schematic representation and (b) portion of a single cationic Ag−Hdpma 4_1-helix chain. Selected bond lengths (Å) and angles (deg): Ag1−N2, 2.173(2); Ag1−N2#1, 2.173(2); N2−Ag1−N2#1, 173.34(11). Symmetry code: #1, $-y + {}^5/_4$, $-x + {}^5/_4$, $-z + {}^1/_4$. (c) Top- and (d) side-view of the 5-fold interweaved homochiral 4_1-helices. Nitrate anions, lattice water molecules, and carbon-bound hydrogen atoms are omitted for clarity.

dx.doi.org/10.1021/ic500306y | Inorg. Chem. 2014, 53, 5581−5588

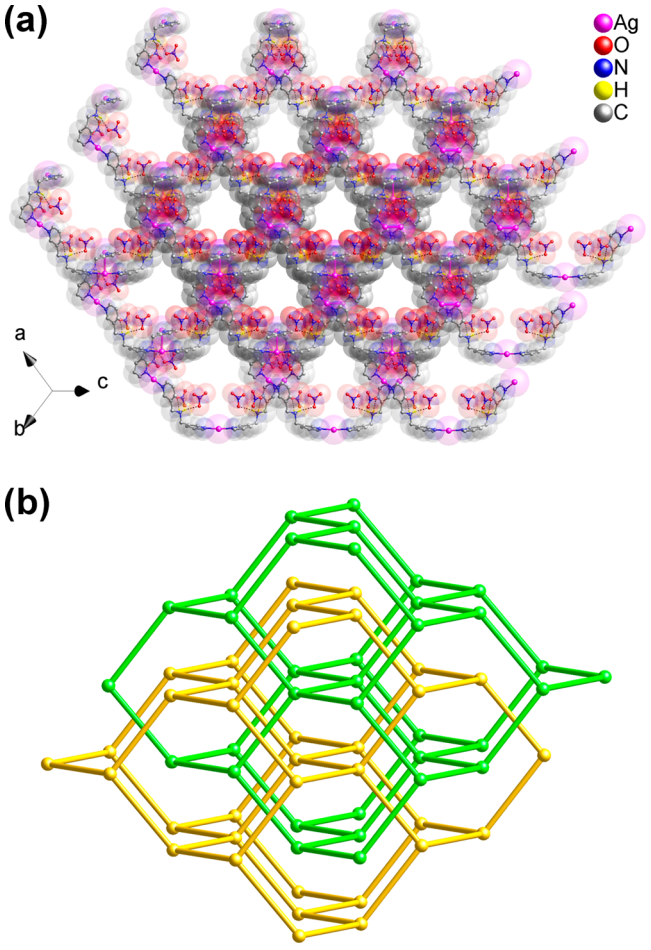

Figure 2. (a) Single network structure of **1**, showing one-dimensional open channels. (b) Topological view of the 2-fold interpenetrating diamondoid-like nets in **1**.

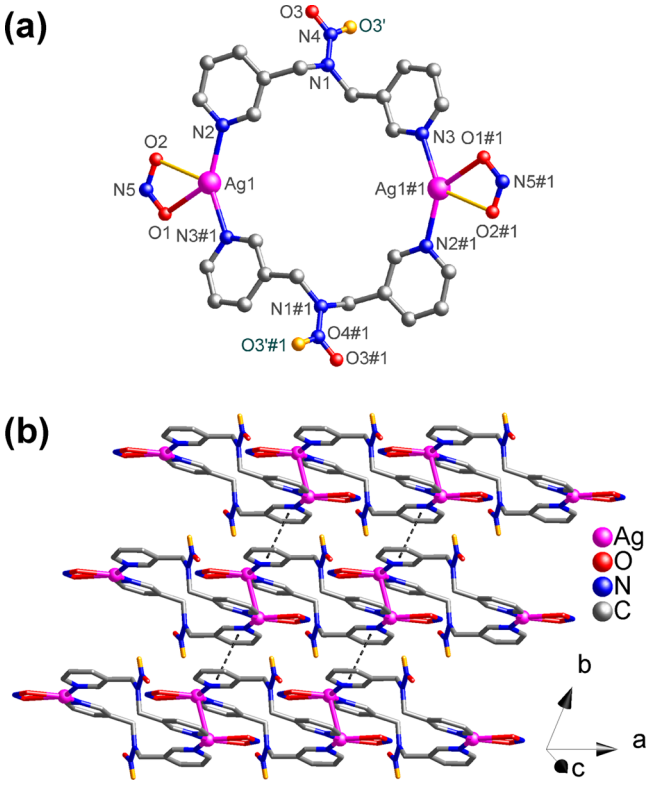

Figure 3. (a) Molecular loop structure of **2**. Selected bond lengths (Å) and angles (deg): Ag1−N2, 2.229(2); Ag1−N3#1, 2.260(2); Ag1−O1, 2.421(2); Ag1−O2, 2.68; N1−N4, 1.325(3); N2−Ag1−N3#1, 135.57(8); O1−Ag1−N2, 135.81(8); O1−Ag1−N3#1, 88.02(8). Symmetry code: #1, $-x + 2, -y, -z$. (b) Intermolecular argentophilic (pink lines, 3.0941(5) Å) and $\pi\cdots\pi$ (black dashed lines, 3.62 Å) interactions supported two-dimensional supramolecular layer array of **2**. Disordered minor part of the *N*-nitroso oxygens are shown in light-orange color.

units with opposite chiralities interpenetrate in a single crystal, yielding a meso compound (Figure 2b and Supporting Information Figure S7). Even with this interpenetration, free void spaces represent about 6.4% of the volume,[23] in which the lattice water molecules reside, forming hydrogen bonds with the nitrate anions (O4−H102···O1, 2.884(14) Å, Supporting Information Figure S7).

In helix **1**, the nitrate anions in the channels come into contact with the host structure via weak Ag···nitrate and noncovalent hydrogen bonding interactions, so the possibility that nitrates could be exchanged with other anions is of interest. An anion-exchange reaction of helix **1** with $NaNO_2$ was performed by immersing a powdered sample of **1** in an aqueous solution of $NaNO_2$ and leaving the solution for about 7 days. The structure of thus obtained colorless crystals was determined as $[Ag(dpma\text{-}NO)(NO_2)]_2$ (**2**) by single-crystal X-ray diffraction analysis and characterized by NMR, IR, and electrospray ionization (ESI) mass spectroscopy. As shown in Figure 3a, compound **2** is clearly an *N*-nitroso compound and crystallizes in the triclinic space group $P\bar{1}$. In the asymmetric unit, there is one silver atom, one *N*-nitrosated dpma-NO ligand, and one nitrite anion. The dpma-NO ligand has a gauche−gauche−syn conformation, with $C_{py}-C-N_{am}-C$ torsion angles of −91.3° and −81.5°, and coordination to two Ag atoms. The N1(amine)−N4(nitrosyl) bond length is 1.325(3) Å, which is shorter than that of an N−N single bond (1.42 Å) and falls within the range 1.31−1.34 Å for most of organic nitrosamines R_2NNO (where the NNO moiety is linked to two sp^3-hybridized carbon atoms).[24] Accordingly, this bond length corresponds to a partial N═N double bond, which arises from the contribution of the dipolar resonance form (Supporting Information Chart S1), which is one of the two Lewis representations of nitrosamines. However, the *N*-nitroso oxygen is disordered in two positions, with refined occupancies of 0.6:0.4, such that the major and the minor parts are cisoid with trans- and gauche-configured 3-picolyl groups, respectively, most likely because of the steric hindrance by the methylene hydrogen. The Ag atom is three-coordinated by two pyridine nitrogens of two dpma-NO ligands and one oxygen of nitrite anion, generating a distorted trigonal planar geometry (N−Ag−N/O, 88.02(8)−135.81(8)°). In fact, the second oxygen of the nitrite anion is in weak contact with the Ag atom with a relatively long Ag···O distance of 2.68 Å. Compound **2** forms a chairlike M_2L_2 molecular loop structure (Figure 3a), with a Ag···Ag separation of 9.18 Å. These molecular loops stack well along the crystallographic *a* axis, with an intermolecular argentophilic interaction of 3.0941(5) Å, to generate an infinite chain array, which is in the form of a row of fused loops. This chain then interacts with another via $\pi\cdots\pi$ interactions (3.62 Å) between the closed pyridine rings, forming a two-dimensional supramolecular layer array (Figure 3b).

dx.doi.org/10.1021/ic500306y | *Inorg. Chem.* 2014, 53, 5581−5588

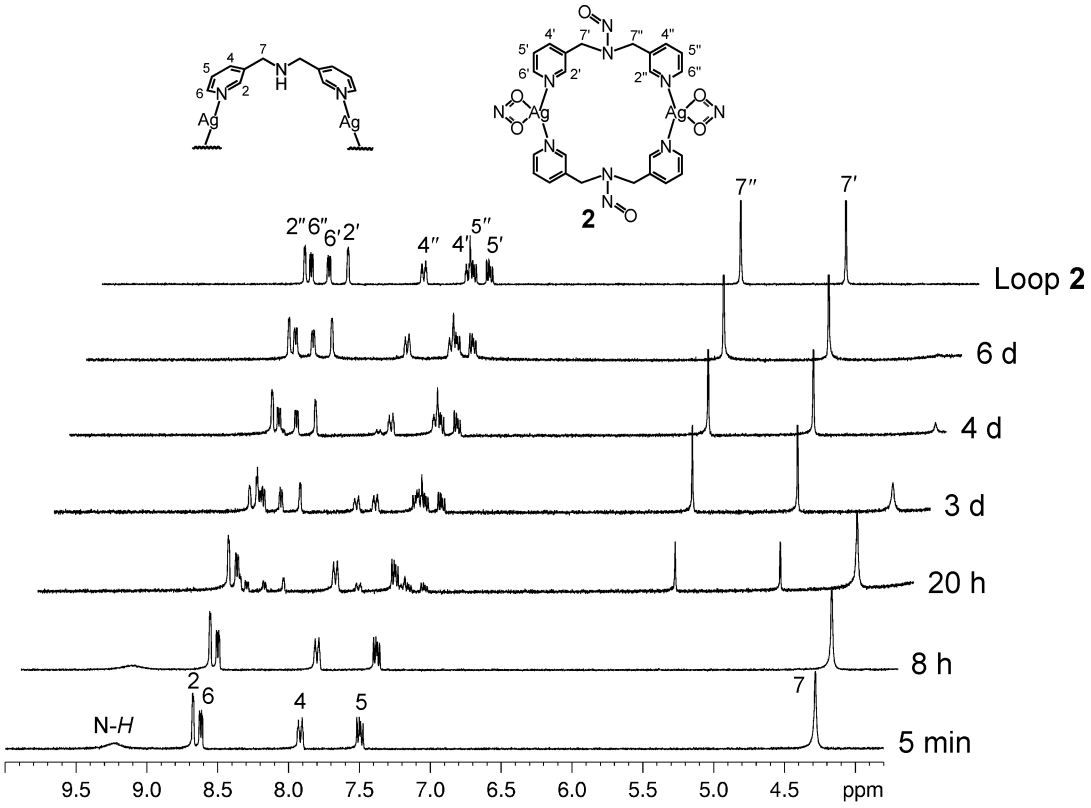

Figure 4. ^{1}H NMR spectra of helix **1** immersed in an aqueous solution of $NaNO_2$ at room temperature for 5 min, 8 h, 20 h, 3 days, 4 days, and 6 days, and of molecular loop **2** (bottom to top).

NMR spectroscopy is a useful tool for studying the configurations of nitrosamines in solution. The room-temperature ^{1}H NMR spectrum of **2** in DMSO-d_6 is particularly notable (Figure 4 and Supporting Information Figure S8), as it includes two sets of remarkably sharp resonances of equal intensity, which correspond to the two 3-picolyl groups of the *N*-nitrosated dpma-NO ligand. The ^{13}C{^{1}H} NMR spectrum of **2** is similar (Supporting Information Figure S10). These spectra most likely follow from the hindrance of the rotation of the nitrosyl group about the N−NO partial double bond.[11,13a] In the ^{1}H NMR spectrum of **2**, the two sets of resonances of 3-picolyl groups are separated by a chemical shift of 0.74 ppm for the α-CH_2 group and 0.12−0.36 ppm for the 3-pyridyl group. The first set of proton signals ($H_{2'}$, $H_{4'}$, $H_{5'}$, $H_{6'}$, and $H_{7'}$) with relative upfield chemical shifts is assigned to the 3-picolyl group that is positioned cis to the nitroso O atom, and the second downfield set ($H_{2''}$, $H_{4''}$, $H_{5''}$, $H_{6''}$, and $H_{7''}$) is assigned to the 3-picolyl group that is positioned trans to the nitroso O atom.[24,25] On the basis of these NMR studies herein, the configuration of the R_2NNO moiety of dpma-NO must be planar, or nearly planar, and only a single isomer in solution is reasonably suggested to have a rotational rate that is slower than the NMR time scale, owing to the high rotational barrier of roughly 18−23 kcal mol^{-1},[26] even though the *N*-nitroso group exhibits orientational disorder in the solid-state. Furthermore, the ^{15}N{^{1}H} NMR spectrum of ^{15}N-labeled compound **2′**, obtained from the anion-exchange reaction of helix **1** with $Na^{15}NO_2$, revealed ^{15}N chemical shifts at 158.951 and 210.017 ppm versus CH_3NO_2 (Supporting Information Figure S12). The former shift is in the range that has been previously reported for *N*-nitrosamines,[26a,27] whereas the latter is assigned to the nitrite anion that is bound to the Ag^{I} ion. This finding verifies that the nitroso group came from the nitrite anion and actually is functionalized on the amine group of dpma-NO ligand in **2**.

The ESI mass spectrum of **2** in DMSO solution exhibits major peaks at *m*/*z* 870.9, 718.0, 563.1, 489.9, 460.9, 335.0, and 305.0, masses that correspond to $[M + Ag]^+$ (calcd *m*/*z* 870.9), $[M - NO_2]^+$ (calcd *m*/*z* 718.0), $[M - 2NO_2 - Ag]^+$ (calcd *m*/*z* 563.1), $[M - NO_2 - (dpma\text{-}NO)]^+$ (calcd *m*/*z* 489.9), $[M - NO_2 - (dpma\text{-}NO) - NO + H]^+$ (calcd *m*/*z* 460.9), $[M/2 - NO_2]^+$ (calcd *m*/*z* 335.0), and $[M/2 - NO_2 - NO]^+$ (calcd *m*/*z* 305.0), respectively, where M = molecular mass of **2** and the *m*/*z* value is given for the highest isotope line in daltons (Supporting Information Figure S21). The ESI mass spectrum of **2′** shows the shifts in *m*/*z* (874.9, 721.0, 565.1, 491.9, 461.9, 336.0, and 307.0) expected for the $\Delta m/z$ values of $^{14}NO/^{14}NO_2$ versus $^{15}NO/^{15}NO_2$ (Supporting Information Figure S22). These data suggest that the loop structures of **2** and **2′** are retained in solution. The IR spectra of **2** and **2′** are comparable: the spectrum of **2** includes characteristic but weak N═O stretching band at 1456 cm^{-1} and the characteristic antisymmetric N—O stretching band at 1195 cm^{-1}; these signals are shifted to 1410 and 1177 cm^{-1}, respectively, for **2′** (Figure 5), revealing a significant isotope effect.[11,14c,27,28] Therefore, the nitrite (NO_2^-) anion is verified by the nitrosating agent herein, that it is a source of the nitrosonium ion (NO^+), which exhibits the NO functionality to form the final product, *N*-nitrosated amine, as supported by the ESI-MS analyses and IR data.

To understand the processes that are involved in the single-crystal-to-single-crystal (SCSC) structural transformation from helix **1** to molecular loop **2**, the powdered samples prepared by immersing helix **1** in an aqueous solution of $NaNO_2$ were time-dependently isolated, and then characterized by ^{1}H NMR and

dx.doi.org/10.1021/ic500306y | *Inorg. Chem.* 2014, 53, 5581−5588

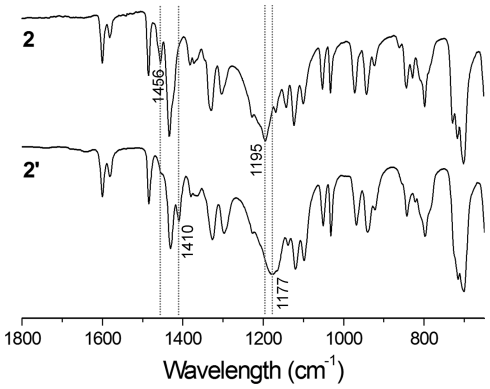

Figure 5. Comparison of partial IR spectra of molecular loops **2** (top) and **2′** (down).

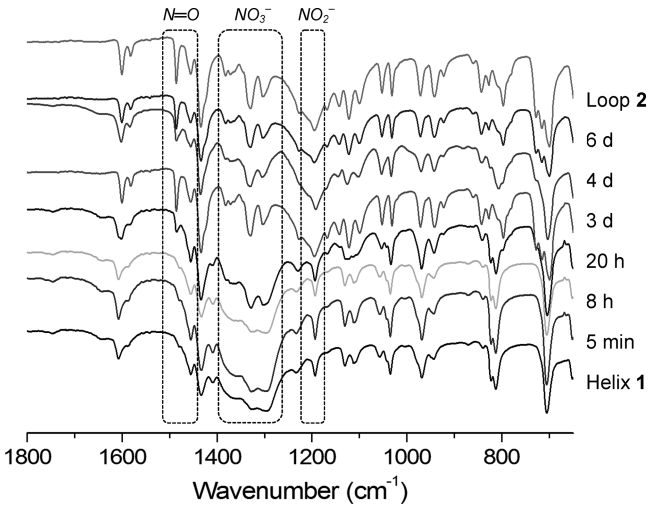

Figure 6. Partial IR spectra of helix **1**, of the powdered samples obtained by immersing **1** in an aqueous solution of $NaNO_2$ at room temperature for 5 min, 8 h, 20 h, 3 days, 4 days, and 6 days, and of molecular loop **2** (bottom to top).

IR spectroscopies. As shown in Figure 4, the ^{1}H NMR spectra of the powdered samples obtained after immersion for 5 min and 8 h are identical, and reveal a single set of four pyridine and one methylene sharp peaks of 3-picolyl groups, differing greatly from the spectrum of molecular loop **2**. These proton signals were shifted downfield by ∼0.16 and 0.61 ppm for 3-pyridyl and methylene protons, respectively, from those of the "free" ligands,[17] indicative of coordination between silver(I) and dpma by the metal induction effect.[29] Notably, a ^{1}H NMR spectrum with almost identical resonances was also observed when helix **1** was immersed in DMSO-d_6 for 1 day (Supporting Information Figure S13). These observations suggest several facts: (a) the collapse of the polymeric structure of helix **1** in DMSO solution forms a single solution species of Ag−dpma complexation, which may have a cyclic structure, or a mixture of multiple potential complexation motifs that are rapidly interconverted to establish a dynamic equilibrium on the NMR time-scale owing to the labile silver−ligand bond,[18,29] (b) the presence of a nitrite anion promotes this collapse process, and (c) *N*-nitrosation of dpma ligand and anion-exchange do not happen at this time. However, the ^{1}H NMR spectrum of the powdered sample that was obtained following their immersion for ∼20 h revealed that the N*H* signal (δ 9.32 ppm) disappeared, and at the same time, a new pattern including two sets of separate 3-picolyl resonances of equal intensity that is identical to the spectrum of molecular loop **2** appeared. Obviously, anion-exchange and *N*-nitrosation on the dpma ligand have been achieved simultaneously. After ∼6 days, the solid-state structural transformation from helix **1** to molecular loop **2** was complete.

The IR spectra agree with the NMR results that were discussed above. As shown in Figure 6, the IR spectra of the powdered samples that were obtained by the immersion of **1** in an aqueous solution of $NaNO_2$ do not differ significantly from that of **1**, until about 20 h of immersion, when the characteristic NO_3^- peaks ($\nu \approx$ 1355 and 1296 cm^{-1}) were weakened. In 6 days, the complete disappearance of the characteristic NO_3^- peaks and the emergence of the characteristic NO_2^- peak ($\nu \approx$ 1195 cm^{-1}) and the characteristic N=O stretching band ($\nu \approx$ 1456 cm^{-1}) reveal that not only is the NO_3^- anion quantitatively displaced by the NO_2^- anion, but also the dpma ligand is *N*-nitrosated to become the dpma-NO ligand.

Scanning electron microscopy (SEM) was used to visualize the influence of the structural transformation on the morphology of the materials because it captures images of the nanoscopic features on the crystal surface. In this study, SEM images reveal that the surfaces of crystals of **1** change remarkably when they are immersed in an aqueous solution of $NaNO_2$ (Supporting Information Figure S20). After several hours of immersion, the relatively flat surface of the single crystal is slightly rough, suggesting that the crystal has begun to undergo a restructuring. A clear restructuring of the crystal surface is observed following immersion for 20 h to 4 days, as verified by the bumpy crystal surface and, perhaps, the formation of new crystal phases on the surface of the single crystal. The restructuring continues until the final surface of the single crystal has become more regular. Therefore, SEM images indicate significant transformations in the crystal surface profile that are consistent with the time-dependent ^{1}H NMR and IR measurements (Figures 4 and 6).

The results of the ^{1}H NMR and IR analyses suggest the formation of an intermediate, which should be a high-symmetry nitrate-containing species, before the ligand *N*-nitrosation. To gain more information on the structural integrity of the postulated intermediate in solution, an ESI mass spectrum of the powdered sample that was obtained by immersion of **1** in an aqueous solution of $NaNO_2$ for 3 h was carried out (Supporting Information Figure S23). The mass spectrum includes three main peaks that correspond to $[Ag_2(dpma)_2(NO_3)]^+$ (m/z 676.0), $[Ag_2(dpma)(NO_3)]^+$ (m/z 476.9), and $[Ag(dpma)]^+$ (m/z 306.0), respectively, and two relatively weak peaks that correspond to $[Ag_2(dpma)_2(NO_3)_2 + Ag]^+$ (m/z 844.9) and $[Ag(dpma)_2]^+$ (m/z 507.1). All of these peaks reasonably suggest a single nitrate-containing intermediate that has the formula $[Ag(dpma)(NO_3)]_2$ (**I**) and has a molecular loop structure.

Interestingly, recrystallization of intermediate **I** in water would regenerate the crystal phase of **1**. In a parallel experiment, the recrystallization of intermediate **I** from an aqueous solution of excess sodium nitrite formed molecular loop **2**, suggesting that the SCSC structural transformation from helix **1** to molecular loop **2** is a two-step process: nitrite-induced structural transformation followed by anion exchange/*N*-nitrosation.

On the basis of NMR, ESI-MS, and IR spectra data and recrystallization studies, Scheme 1 is postulated as the SCSC

dx.doi.org/10.1021/ic500306y | Inorg. Chem. 2014, 53, 5581−5588

Scheme 1. Postulated Convertion Process of SCSC Structural Transformation from Helix 1 to Molecular Loop 2

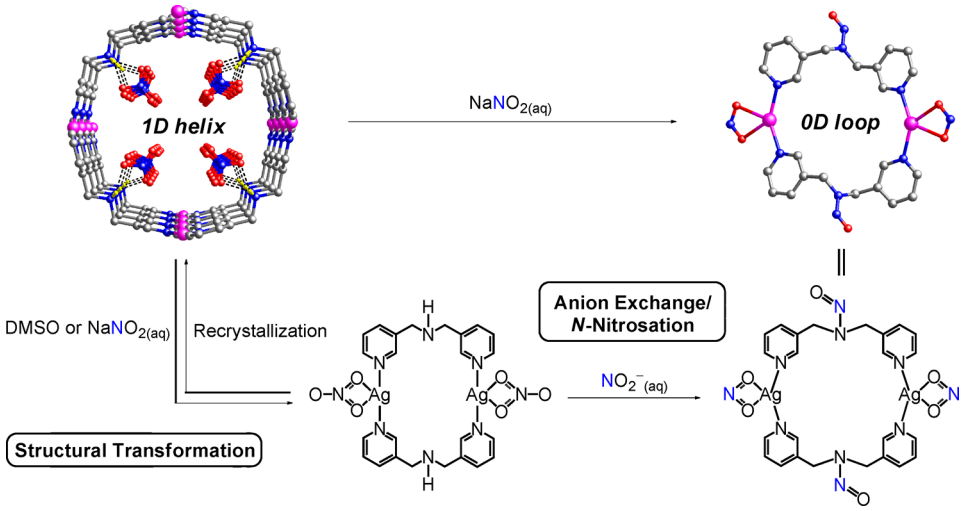

structural transformation. First, crystalline samples of helix **1** immersed in an aqueous solution of nitrite anions are destroyed, reforming a nitrate-containing intermediate **I** with a dinuclear loop structure, via a nitrite-induced structural transformation. Then, the intermediate **I** is converted to the final nitrite-containing *N*-nitrosated product molecular loop **2**, by an anion-exchange that is associated with ligand *N*-nitrosation.

Another anion exchange that involves remarkable structural transformation was observed when the powdered sample of helix **1** was immersed into an aqueous solution of tetra-*n*-butylammonium fluoride (TBAF) and left undisturbed at room temperature for 1 week. The colorless crystalline product thus obtained is identified as $[Ag(dpma)(H_2O)](NO_3)$, which can be found in the literature and, according to the literature, has a one-dimensional polymeric structure that resembles a topological binodal ladder chain with Ag and dpma both as three-connected T-nodes (Supporting Information Figure S24).[18] This effect may be attributed to the essential basicity of the F^- anion that is capable of abstraction of the ammonium proton, causing a drastic SCSC structural transformation from the 1D helix chain of **1** to the 1D ladder-like chain of $[Ag(dpma)(H_2O)](NO_3)$.

The thermogravimetric (TG) trace of **1** reveals a gradual weight loss during heating from room temperature to 105 °C (Supporting Information Figure S25), corresponding to the escape of the lattice water molecules (found 3.8%, calcd 4.0%). The solvent-free coordination framework is then retained up to ca. 225 °C, above which temperature it abruptly decomposes. The final residue is likely that of Ag (found 24.3% at $T \approx 465$ °C, calcd 24.0%). The TG curve of **2** is largely unchanged up to 180 °C, above which temperature it abruptly decomposes. The final residue is likely that of Ag (found 28.9%, calcd 28.2%).

The room-temperature solid-state luminescent spectra (λ_{ex} = 240 nm) of **1**, **I**, and **2** exhibit similar purple-blue emission bands that are centered at 401, 403, and 411 nm, respectively (Supporting Information Figure S26), whereas compound $[Ag(dpma)(H_2O)](NO_3)$ has an emission band at 408 nm.[18] These bands compare well with that of the dpma ligand which in acetonitrile solution exhibits an extremely weak room-temperature emission band at ~434 nm,[18] meaning that the complexation of the free dpma ligand into the Ag-based compounds significantly blue-shifts its emission.

CONCLUSION

In summary, this work presents a fascinating 5-fold interweaved 1D helix structure that resembles a 3D topological diamondoid-like net through the connections of ligand-unsupported helix-to-helix argentophilic interactions. Two identical diamondoid-like nets with opposite chiralities interpenetrate in a single crystal to produce a meso compound. Anion-exchange reactions cause a remarkable SCSC structural transformation from the 1D helix to the 0D molecular loop (induced by the nitrite anion) and a 1D molecular ladder (induced by the fluoride anion). Most importantly, this work is the first to present observations of an unexpected nitrite-dominated in situ *N*-nitrosation of an amine ligand along with the aforementioned SCSC structural transformation in inorganic supramolecular chemistry.

ASSOCIATED CONTENT

Supporting Information

X-ray crystallographic data in CIF format; XRPD patterns; additional structural figures; NMR, IR, ESI-MS, TGA, and photoluminescence spectra; SEM images. This material is available free of charge via the Internet at http://pubs.acs.org.

AUTHOR INFORMATION

Corresponding Author

*E-mail: jyunwu@ncnu.edu.tw.

Notes

The authors declare no competing financial interest.

ACKNOWLEDGMENTS

We are grateful for the financial aid from the National Chi Nan University and the Ministry of Science and Technology of Taiwan.

REFERENCES

(1) See some recent reviews: (a) O'Keeffe, M.; Yaghi, O. M. *Chem. Rev.* **2012**, *112*, 675−702. (b) Perry, J. J., IV; Perman, J. A.; Zaworotko, M. J. *Chem. Soc. Rev.* **2009**, *38*, 1400−1417. (c) D'Alessandro, D. M.; Smit, B.; Long, J. R. *Angew. Chem., Int. Ed.* **2010**, *49*, 6058−6082. (d) Li, J.-R.; Sculley, J.; Zhou, H.-C. *Chem. Rev.* **2012**, *112*, 869−932. (e) Fu, Y.; Sun, D.; Chen, Y.; Huang, R.; Ding, Z.; Fu, X.; Li, Z. *Angew. Chem., Int. Ed.* **2012**, *51*, 3364−3367.

(f) Yoon, M.; Srirambalaji, R.; Kim, K. *Chem. Rev.* **2012**, *112*, 1196−1231.
(2) (a) Farrusseng, D.; Aguado, S.; Pinel, C. *Angew. Chem., Int. Ed.* **2009**, *48*, 7502−7513. (b) Ma, L.; Falkowski, J. M.; Abney, C.; Lin, W. *Nat. Chem.* **2010**, *2*, 838−846. (c) Kreno, L. E.; Leong, K.; Farha, O. K.; Allendorf, M.; van Duyne, R. P.; Hupp, J. T. *Chem. Rev.* **2012**, *112*, 1105−1125. (d) Thanasekaran, P.; Luo, T. T.; Lee, C. H.; Lu, K. L. *J. Mater. Chem.* **2011**, *21*, 13140−13149.
(3) (a) Li, G.; Yu, W.; Cui, Y. *J. Am. Chem. Soc.* **2008**, *130*, 4582−4583. (b) Bradshaw, D.; Prior, T. J.; Cussen, E. J.; Claridge, J. B.; Rosseinsky, M. J. *J. Am. Chem. Soc.* **2004**, *126*, 6106−6114. (c) Wu, C.-D.; Hu, A.; Zhang, L.; Lin, W. *J. Am. Chem. Soc.* **2005**, *127*, 8940−8941. (d) Tanaka, K.; Oda, S.; Shiro, M. *Chem. Commun.* **2008**, 820−822. (e) Seo, J. S.; Whang, D.; Lee, H.; Jun, S. I.; Oh, J.; Jeon, Y. J.; Kim, K. *Nature* **2000**, *404*, 982−986.
(4) See some examples: (a) Zheng, X.-D.; Lu, T.-B. *CrystEngComm* **2010**, *12*, 324−336 and references cited therein. (b) Han, L.; Hong, M. *Inorg. Chem. Commun.* **2005**, *8*, 406−419. (c) McMorran, D. A. *Inorg. Chem.* **2008**, *47*, 592−601. (d) Jung, O.-S.; Kim, Y. J.; Lee, Y.-A.; Park, J. K.; Chae, H. K. *J. Am. Chem. Soc.* **2000**, *122*, 9921−9925. (e) Wu, J.-Y.; Huang, S.-M. *CrystEngComm* **2011**, *13*, 2062−2070. (f) Chen, X.-D.; Du, M.; Mak, T. C. W. *Chem. Commun.* **2005**, 4417−4419.
(5) (a) Wei, W.; Yu, H.; Jiang, F.; Liu, B.; Ma, J.; Hong, M. *CrystEngComm* **2012**, *14*, 1693−1700. (b) Cui, X.; Khlobystov, A. N.; Chen, X.; Marsh, D. H.; Blake, A. J.; Lewis, W.; Champness, N. R.; Roberts, C. J.; Schröder, M. *Chem.—Eur. J.* **2009**, *15*, 8861−8873. (c) Min, K. S.; Suh, M. P. *J. Am. Chem. Soc.* **2000**, *122*, 6834−6840. (d) Du, M.; Zhao, X.-J.; Guo, J.-H.; Batten, S. R. *Chem. Commun.* **2005**, 4836−4838.
(6) (a) Ferreira, I. M. P. L. V. O.; Silva, S. *Talanta* **2008**, *74*, 1598−1602. (b) Moorcroft, M. J.; Davis, J.; Compton, R. G. *Talanta* **2001**, *54*, 785−803. (c) Rau, J.-R.; Chen, S.-C.; Sun, H.-W. *Electrochim. Acta* **1994**, *39*, 2773−2779. (d) Osterloh, J.; Goldfield, D. *J. Liq. Chromatogr. Relat. Technol.* **1984**, *7*, 753−763.
(7) (a) Meng, H.-B.; Wang, T.-R.; Guo, B.-Y.; Hashi, Y.; Guo, C.-X.; Lin, J.-M. *Talanta* **2008**, *76*, 241−245. (b) Gapper, L. W.; Fong, B. Y.; Otter, D. E.; Indyk, H. E.; Woollard, D. C. *Int. Dairy J.* **2004**, *14*, 881−887.
(8) (a) Noro, S.-i.; Kitaura, R.; Kondo, M.; Kitagawa, S.; Ishii, T.; Matsuzaka, H.; Yamashita, M. *J. Am. Chem. Soc.* **2002**, *124*, 2568−2583. (b) Min, K. S.; Suh, M. P. *J. Am. Chem. Soc.* **2000**, *122*, 6834−6840. (c) Luo, T.-T.; Liu, Y.-H.; Chan, C.-C.; Huang, S.-M.; Chang, B.-C.; Lu, Y.-L.; Lee, G.-H.; Peng, S.-M.; Wang, J.-C.; Lu, K.-L. *Inorg. Chem.* **2007**, *46*, 10044−10046.
(9) See some examples: (a) Kole, G. K.; Vittal, J. J. *Chem. Soc. Rev.* **2013**, *42*, 1755−1775 and references cited therein. (b) Dou, L.; Zheng, Y.; Shen, X.; Wu, G.; Fields, K.; Hsu, W.-C.; Zhou, H.; Yang, Y.; Wudl, F. *Science* **2014**, *343*, 272−277. (c) Bushuyev, O. S.; Tomberg, A.; Friščšć, T.; Barrett, C. J. *J. Am. Chem. Soc.* **2013**, *135*, 12556−12559. (d) Choi, H. J.; Suh, M. P. *J. Am. Chem. Soc.* **2004**, *126*, 15844−15851. (e) Legrand, Y.-M.; van der Lee, A.; Masquelez, N.; Rabu, P.; Barboiu, M. *Inorg. Chem.* **2007**, *46*, 9083−9089. (f) Hu, C.; Englert, U. *Angew. Chem., Int. Ed.* **2006**, *45*, 3457−3459. (g) Ding, N.; Kanatzidis, M. G. *Angew. Chem., Int. Ed.* **2006**, *45*, 1397−1401. (h) Das, S.; Kim, H.; Kim, K. *J. Am. Chem. Soc.* **2009**, *131*, 3814−3815.
(10) (a) Kitagawa, S.; Kitaura, R.; Noro, S.-i. *Angew. Chem., Int. Ed.* **2004**, *43*, 2334−2375. (b) Uemura, K.; Matsuda, R.; Kitagawa, S. *J. Solid State Chem.* **2005**, *178*, 2420−2429.
(11) Wang, P. G.; Xian, M.; Tang, X.; Wu, X.; Wen, Z.; Cai, T.; Janczuk, A. J. *Chem. Rev.* **2002**, *102*, 1091−1134.
(12) (a) Gladwin, M. T.; Schechter, A. N.; Kim-Shapiro, D. B.; Patel, R. P.; Hogg, N.; Shiva, S.; Cannon, R. O., III; Kelm, M.; Wink, D. A.; Espey, M. G.; Oldfield, E. H.; Pluta, R. M.; Freeman, B. A.; Lancaster, J. R., Jr.; Feelisch, M.; Lundberg, J. O. *Nat. Chem. Biol.* **2005**, *1*, 308−314. (b) Loeppky, R. N.; Tomasik, W.; Kerride, B. E. *Carcinogenesis* **1987**, *8*, 941−946. (c) Lijinsky, W. *Chemistry and Biology of N-Nitroso Compounds*; Cambridge University Press: Cambridge, 1992. (d) Lippton, H. L.; Gruetter, C. A.; Ignarro, L. J.; Meyer, R. L.; Kadowitz, P. J. *Can. J. Physiol. Pharmacol.* **1982**, *60*, 68−75. (e) DeRubertis, F. R.; Craven, P. A. *Science* **1976**, *193*, 897−899.
(13) (a) Olszewska, T.; Milewska, M. J.; Gdaniec, M.; Małuszynska, H.; Połonski, T. *J. Org. Chem.* **2001**, *66*, 501−506. (b) Seebach, D.; Enders, D. *Angew. Chem., Int. Ed. Engl.* **1975**, *14*, 15−32. (c) Seebach, D.; Enders, D.; Renger, B. *Chem. Ber.* **1977**, *110*, 1852−1865. (d) Renger, B.; Kalinowski, H.-O.; Seebach, D. *Chem. Ber.* **1977**, *110*, 1866−1878.
(14) (a) Połonski, T.; Pham, M.; Gdaniec, M. *J. Org. Chem.* **1996**, *61*, 3766−3772. (b) Gdaniec, M.; Milewska, M. J.; Połonski, T. *J. Org. Chem.* **1995**, *60*, 7411−7418. (c) Looney, C. E.; Phillips, W. D.; Reilly, E. L. *J. Am. Chem. Soc.* **1957**, *79*, 6136−6142.
(15) (a) Lim, M. H.; Xu, D.; Lippard, S. J. *Nat. Chem. Biol.* **2006**, *2*, 375−380. (b) Nagano, T.; Yoshimura, T. *Chem. Rev.* **2002**, *102*, 1235−1270.
(16) (a) Ohwada, T.; Miura, M.; Tanaka, H.; Sakamoto, S.; Yamaguchi, K.; Ikeda, H.; Inagaki, S. *J. Am. Chem. Soc.* **2001**, *123*, 10164−10172. (b) Tanno, M.; Sueyoshi, S.; Miyata, N.; Nakagawa, S. *Chem. Pharm. Bull.* **1996**, *44*, 1849−1852. (c) Tanno, M.; Sueyoshi, S.; Miyata, N.; Umehara, K. *Chem. Pharm. Bull.* **1997**, *45*, 595−598. (d) Cheng, J.-P.; Xian, M.; Wang, K.; Zhu, X.; Yin, Z.; Wang, P. G. *J. Am. Chem. Soc.* **1998**, *120*, 10266−10267.
(17) Wu, J.-Y.; Zhong, M.-S.; Chiang, M.-H.; Tsai, M.-R.; Lai, L.-L. *Dalton Trans.* **2012**, *41*, 156−164.
(18) Wu, J.-Y.; Chao, T.-C.; Zhong, M.-S. *Cryst. Growth Des.* **2013**, *13*, 2953−2964.
(19) Sheldrick, G. M. *SHELX-97 (Including SHELXS and SHELXL)*; University of Göttingen: Göttingen, Germany, 1997.
(20) Altomare, A.; Cascarano, G.; Giacovazzo, C.; Guagliardi, A. *J. Appl. Crystallogr.* **1993**, *26*, 343−350.
(21) *WINGX*: Farrugia, L. J. *J. Appl. Crystallogr.* **1999**, *32*, 837−838.
(22) Bondi, A. *J. Phys. Chem.* **1964**, *68*, 441−451.
(23) Spek, A. L. *PLATON, A Multipurpose Crystallographic Tool*; Utrecht University: Utrecht, The Netherlands, 2005.
(24) Lee, J.; Chen, L.; West, A. H.; Richter-Addo, G. B. *Chem. Rev.* **2002**, *102*, 1019−1065.
(25) Karabatsos, G. J.; Taller, R. A. *J. Am. Chem. Soc.* **1964**, *86*, 4373−4378.
(26) (a) Karaghiosoff, K.; Klapötke, T. M.; Mayer, P.; Piotrowski, H.; Polborn, K.; Willer, R. L.; Weigand, J. J. *J. Org. Chem.* **2006**, *71*, 1295−1305. (b) Lunazzi, L.; Cerioni, G.; Ingold, K. U. *J. Am. Chem. Soc.* **1976**, *98*, 7484−7488.
(27) Bonnett, R.; Holleyhead, R.; Johnson, B. L.; Randall, E. W. *J. Chem. Soc., Perkin 1* **1975**, *22*, 2261−2264.
(28) Hayashi, T.; Lin, I.-J.; Chen, Y.; Fee, J. A.; Moënne-Loccoz, P. *J. Am. Chem. Soc.* **2007**, *129*, 14952−14958.
(29) (a) Hannon, M. J.; Painting, C. L.; Plummer, E. A.; Child, L. J.; Alcock, N. W. *Chem.—Eur. J.* **2002**, *8*, 2225−2238. (b) Su, C.-Y.; Cai, Y.-P.; Chen, C.-L.; Smith, M. D.; Kaim, W.; zur Loye, H.-C. *J. Am. Chem. Soc.* **2003**, *125*, 8595−8613.